JACS
JOURNAL OF THE AMERICAN CHEMICAL SOCIETY
Communication
pubs.acs.org/JACS

Size-Dependent Electrocatalytic Reduction of CO_2 over Pd Nanoparticles

Dunfeng Gao,[†,§,∥] Hu Zhou,[‡,∥] Jing Wang,[†,§] Shu Miao,[†] Fan Yang,[†] Guoxiong Wang,*[,†] Jianguo Wang,*[,‡] and Xinhe Bao[†]

[†]State Key Laboratory of Catalysis, Dalian Institute of Chemical Physics, Chinese Academy of Sciences, Dalian 116023, China
[‡]College of Chemical Engineering, Zhejiang University of Technology, Hangzhou 310032, China
[§]University of Chinese Academy of Sciences, Beijing 100039, China

Supporting Information

ABSTRACT: Size effect has been regularly utilized to tune the catalytic activity and selectivity of metal nanoparticles (NPs). Yet, there is a lack of understanding of the size effect in the electrocatalytic reduction of CO_2, an important reaction that couples with intermittent renewable energy storage and carbon cycle utilization. We report here a prominent size-dependent activity/selectivity in the electrocatalytic reduction of CO_2 over differently sized Pd NPs, ranging from 2.4 to 10.3 nm. The Faradaic efficiency for CO production varies from 5.8% at −0.89 V (vs reversible hydrogen electrode) over 10.3 nm NPs to 91.2% over 3.7 nm NPs, along with an 18.4-fold increase in current density. Based on the Gibbs free energy diagrams from density functional theory calculations, the adsorption of CO_2 and the formation of key reaction intermediate COOH* are much easier on edge and corner sites than on terrace sites of Pd NPs. In contrast, the formation of H* for competitive hydrogen evolution reaction is similar on all three sites. A volcano-like curve of the turnover frequency for CO production within the size range suggests that CO_2 adsorption, COOH* formation, and CO* removal during CO_2 reduction can be tuned by varying the size of Pd NPs due to the changing ratio of corner, edge, and terrace sites.

The accelerated depletion of fossil fuel resources leads to increasing accumulation of greenhouse gas, CO_2, in the atmosphere, which raises serious environmental concerns.[1] To reduce our dependence on fossil fuels, renewable energy sources, such as solar and wind energies, are growing up rapidly, but these renewable electricities are difficult to merge into the electricity grid due to their intermittent and local nature, and further expansion is highly limited by a lack of efficient energy storage and conversion techniques.[2] Electrocatalytic reduction of CO_2 to fuel and chemical feedstock, powered by intermittent renewable electricity, is an attractive route for simultaneous conversion of CO_2 and renewable energy sources.[3] However, there are several fundamental challenges in the electrocatalytic reduction of CO_2, such as high overpotential, low Faradaic efficiency due to the competitive hydrogen evolution reaction (HER), etc.[4,5] Key points in addressing these issues are the successive CO_2 adsorption,[6−9] intermediates formation,[10,11] and product removal[12,13] on active sites during the electrocatalytic reaction.

Various metallic electrodes have been screened thoroughly, and it is found that the trends on product composition and distribution are strongly dependent on the binding energy of intermediates on metals.[14] For instance, CO_2 is converted into CO on Au and Ag and into hydrocarbons on Cu due to the adsorption strength of CO* intermediates on metals.[14] Varying the particle size has also shown a size effect on the electrocatalytic reduction of CO_2, where the dependence of Faradaic efficiency and current density on particle size has been observed on Ag,[15] SnO_2,[16] Cu,[17] and Au[18,19] nanoparticles (NPs). However, there have been limited studies looking into the size effect among NPs smaller than 10 nm, which are most commonly used in catalysis. Recently, studies on the CO_2 reduction reactivity trends over Au NPs within a very narrow size range of ∼1−8 nm[18] or 4−10 nm[19] were reported. Current density for both CO and H_2 production increases obviously with decreasing the size of Au NPs along with the decrease in Faradaic efficiency toward CO production. Density functional theory (DFT) calculations reveal that the edge site on Au NPs is much more active than terrace and corner sites for CO_2 reduction to CO, while corner sites are highly active for competitive HER. In contrast to the behavior of Au NPs, we report here Faradaic efficiency for CO production increases with decreasing Pd NP size in a size range of 2.4−10.3 nm, which varies from 5.8% at −0.89 V (vs reversible hydrogen electrode, RHE) over 10.3 nm NPs to 91.2% over 3.7 nm NPs, along with an 18.4-fold increase in current density for CO production. DFT calculations indicate that corner and edge sites (small Pd NPs) facilitate the adsorption of CO_2 and formation of key reaction intermediates COOH* during CO_2 reduction compared with terrace one (large Pd NPs), while the formation of H* for competitive HER is similar on all three sites. Furthermore, a volcano-like curve of the turnover frequency (TOF) for CO production within the size range suggests that CO_2 adsorption, COOH* formation, and CO* removal during CO_2 reduction can be tuned on differently sized Pd NPs due to the changing ratio of corner, edge, and terrace sites.

Received: January 3, 2015
Published: March 6, 2015

DOI: 10.1021/jacs.5b00046
J. Am. Chem. Soc. 2015, 137, 4288−4291

A series of carbon-supported Pd NPs were prepared using sodium citrate as a stabilizing agent and $NaBH_4$ as a reductive agent. The particle size of Pd NPs was controlled by adjusting the ratio of sodium citrate to $PdCl_2$ and the reduction temperature. For distinction, the average size of Pd NPs in each sample was used in the sample name, for instance, 3.7 nm Pd indicates that Pd NPs in the Pd/C catalyst has an average particle size of 3.7 nm. Figure 1 and Figure S1 show

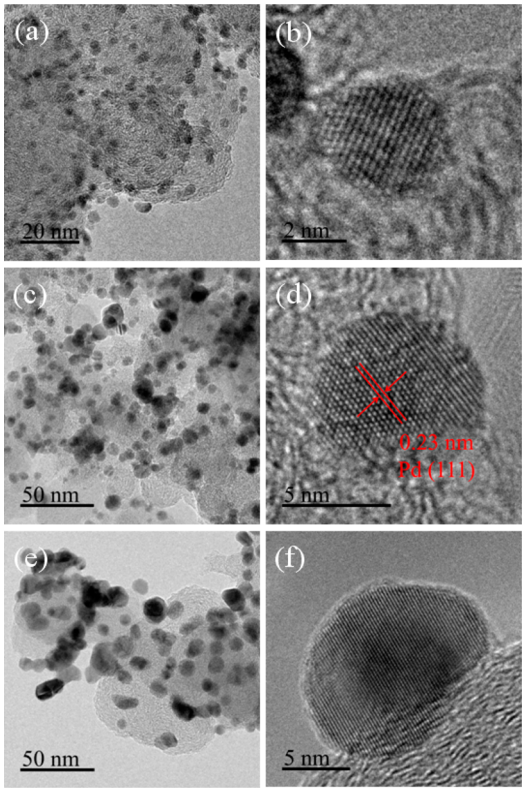

Figure 1. TEM image and HRTEM images of (a,b) 3.7, (c,d) 6.2, and (e,f) 10.3 nm Pd.

transmission electron microscopy (TEM) and high-resolution TEM (HRTEM) images of six Pd/C catalysts with different sizes. The NPs are uniformly deposited on carbon support, and typical Pd(111) plane with the characteristic lattice spacing of 0.23 nm is observed. Figure S2 shows the corresponding histograms of particle-size distribution of six Pd/C catalysts by counting more than 200 particles for each from the TEM images. The particle size distribution gradually broadens with increasing NP size. X-ray diffraction (XRD) patterns of the Pd NPs are shown in Figure S3, and the average crystalline size of Pd NPs was calculated from the (220) diffraction peak (Table S1). Obviously, both TEM and XRD results confirm that a series of Pd NPs in a narrow size range are successfully prepared. The actual loadings of Pd in all the Pd/C catalysts are 18.3 ± 0.5 wt%, as measured by inductively coupled plasma optical emission spectroscopy (ICP-OES) as listed in Table S1. The consistent loading of Pd in Pd/C catalysts allows us to directly compare CO_2 reduction activities of different Pd/C catalysts and investigate the size effect of Pd NPs.

Controlled potential electrolysis of CO_2 was performed in an H-cell (separated by Nafion 115) filled with 0.1 M $KHCO_3$ solution (pH 6.8) as shown in Scheme S1. Under the reported reaction conditions, CO and H_2 were major products as detected by an online micro gas chromatography (GC), and only trace amount of formate with a Faradaic efficiency of 0.37−1.3% (Table S2 and Figure S4) was detected by nuclear magnetic resonance (NMR). Figure 2 shows the applied

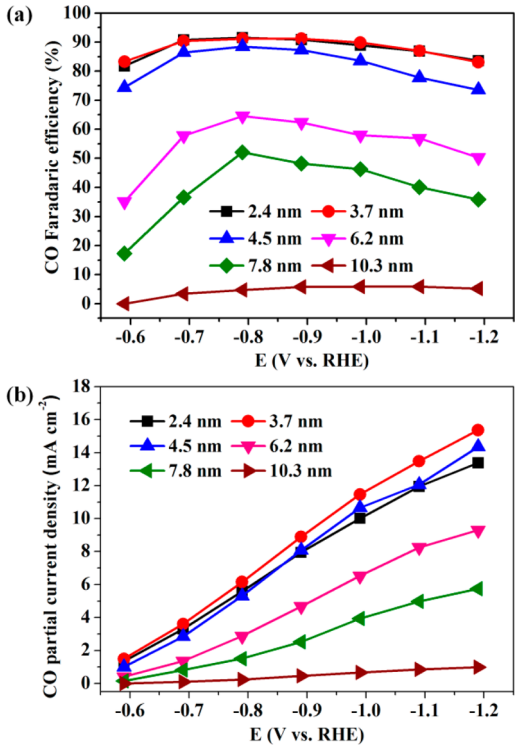

Figure 2. Applied potential dependence of (a) Faradaic efficiencies and (b) current densities for CO production over Pd NPs with different sizes.

potential dependence of Faradaic efficiency and current density for CO production over Pd NPs. All the Faradaic efficiencies for CO production first increase with applied potential, despite the size of Pd NPs. The competitive HER is facile at low overpotentials and CO_2 reduction is prone to occur with increased applied potential. However, the Faradaic efficiency decreases at high applied potentials, which is probably caused by the limited mass transport of CO_2 in 0.1 M $KHCO_3$ solution. On 2.4 and 3.7 nm Pd, all the Faradaic efficiencies at different potentials exceed 80%, and the maximum value of 91.2% is reached at −0.89 V (vs RHE), which is much higher than that over Pd wire electrode (<6%).[20] The Faradaic efficiencies for CO production over 2.4 and 3.7 nm Pd are also comparable to those over Au and Ag NPs.[15,18,19,21]

The current density for CO production increases with applied potential (Figure 2b), indicative of accelerated reaction rate for CO_2 reduction at high applied potentials. Figure S5 summarizes the mass activities of Pd NPs for CO production at various potentials. The mass activity reaches 23.9 A g^{-1}_{Pd} at −0.89 V (vs RHE) on 3.7 nm Pd, which is higher than that on 4 nm Au NPs[19] in the case of a similar metal loading on carbon and is comparable to that on ultrathin Au nanowire.[21] It should be noted that the mass activity of Pd NPs was measured based on gas diffusion electrode, which can be directly used in practical compact electrolysis cells. Therefore, these Pd/C catalysts demonstrate promising applications for practical industrial CO_2 electrocatalytic reduction processes.

DOI: 10.1021/jacs.5b00046
J. Am. Chem. Soc. 2015, 137, 4288−4291

Interestingly, the Faradaic efficiencies and current densities for CO formation over Pd NPs with different sizes are quite different at various potentials. The current densities for CO production on 2.4 nm Pd are smaller than that on 3.7 nm Pd with nearly the same Faradaic efficiency. Further increasing the size of Pd NPs, both Faradaic efficiencies and current densities for CO production decrease saliently. The Faradaic efficiency decreases sharply from 91.2% to 5.8% over a particle size ranging from 3.7 to 10.3 nm at −0.89 V (vs RHE). The current densities for CO production also change in the same trend, and the current density on 3.7 nm Pd has an 18.4-fold increase compared to that over 10.3 nm Pd, which is in contrast to the case of Au NPs.[18,19] To the best of our knowledge, the unique particle size dependence of the Faradaic efficiencies and current densities toward CO_2 reduction has not been reported previously.

In order to understand the relationship between the CO_2 reduction reactivity and the size of Pd NPs, DFT calculations were conducted. It is still a computational challenge to directly simulate the CO_2 reduction over Pd NPs with different sizes by means of DFT calculations. However, it is possible to simulate the process over three different reaction sites (terrace, edge, and corner) of Pd NPs, represented by flat Pd(111) surfaces, stepped Pd(211) surfaces, and Pd55 (or Pd38) clusters, respectively. Furthermore, according to the ratio of three kinds of reaction sites (terrace, edge, and corner) on ideal Pd NPs with different sizes, it is reasonable to build the intrinsic relationship between catalytic properties and NPs size.[22] CO_2 weakly adsorbs on Pd(111), Pd(211), Pd55 with 0.23, −0.11, and −0.21 eV respectively, and CO_2 prefers to be away from Pd(111) (Figure S6). The calculated Gibbs free energy diagrams for CO_2 reduction into CO on Pd(111), Pd(211), Pd55, and Pd38 at 0 V (vs RHE) are shown in Figure 3

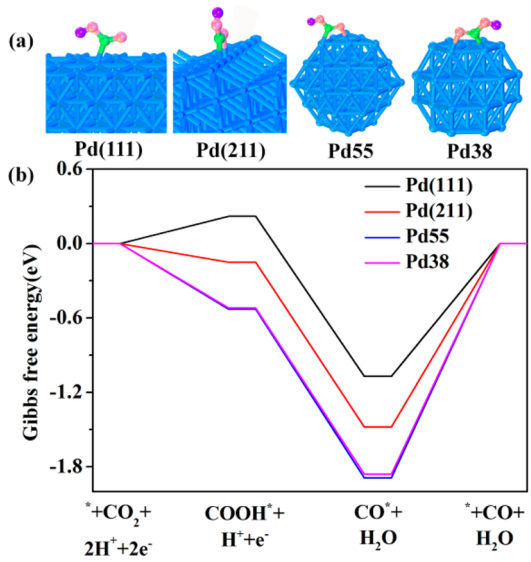

Figure 3. (a) Adsorption of COOH. (b) Free energy diagrams for CO_2 reduction to CO on Pd(111), Pd(211), Pd55, and Pd38.

according to the methodology proposed by Nørskov et al.[23] It is seen that on Pd(111), the formation of COOH*, a key reaction intermediate of CO_2 reduction, is associated with an increase in free energy (0.22 eV), while on Pd(211) and Pd55, COOH* is very stable with a release of −0.15 and −0.53 eV, respectively. Therefore, the formation of reaction intermediate COOH* becomes easier from terrace (Pd(111)), stepped (Pd(211)) to corner (Pd55). Pd38 has a free energy similar to that of Pd55. On these models, the formation of CO*, another reaction intermediate, are all exergonic with Gibbs free energy changes very similar to that of COOH*, because the conversion of COOH* to CO* is typically facile.[21,24] Therefore, it is concluded that the formation of COOH* is a key electrochemical step for CO_2 reduction to CO. The main reason for different changes of Gibbs free energies on different reaction sites is that the adsorption of COOH and CO become stronger from terrace to step to corner site (Figure 3 and Figure S7). These calculations well explain that Pd NPs have positive shifts in the position of the reduction peak of $Pd(OH)_2$ in the cathodic scan[25] between 0.9 and 0.5 V with increasing particle size (Figure S8). The reduction peak potential of $Pd(OH)_2$ shows a linear increase with increasing the size of Pd NPs (Figure S8c), since a stronger hydroxyl adsorption on defects (corner and edge sites), corresponding to small Pd NPs, than on terrace sites for large Pd NPs.[26] The strong adsorption of CO on Pd NPs could be probed by the electrochemical CO stripping voltammetry method.[25] As shown in Figure S9, a broad CO stripping profile with a dominant peak around 1.03 V (vs RHE) occurs on 2.4, 3.7, and 4.5 nm Pd, whereas there is a sharp peak around 0.9 V (vs RHE) with a shoulder peak around 1.03 V (vs RHE) on 6.2, 7.8, and 10.3 nm Pd. The negative shift on peak potential and the reduced current density at 1.03 V (vs RHE) with increasing particle size suggest the weakened adsorption of CO on Pd NPs, in consistent with the DFT calculations (Figure S7). From the calculated Gibbs free energy diagrams, the formation of H_2 has tiny differences on these models (Figure S10), and the overall Gibbs free energy changes is much smaller than that for the formation of CO*, indicating that CO_2 reduction is predominant under the present experimental conditions.

According to the DFT calculation results, the corner and edge sites on Pd NPs are considered active for CO_2 reduction, and the corner, edge, and terrace sites are all active for HER. TOF for CO or H_2 production on Pd NPs at various potentials was calculated according to the ratio of corner and edge or the ratio of corner, edge, and terrace in Pd NPs (Figure S11). Figure 4 shows the size dependence of TOF for CO production at various potentials. The maximum TOF varies from 3.7 to 4.5 nm Pd when the applied potential is shifted from −0.59 to −0.89 V (vs RHE) gradually. The sluggish removal of CO* at a high coverage on 3.7 nm Pd, having a higher ratio of corner and edge sites, probably retards the increase of TOF with the

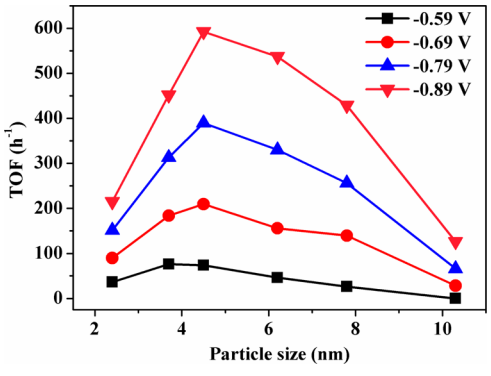

Figure 4. Size dependence of TOF for CO production on Pd NPs at various potentials.

DOI: 10.1021/jacs.5b00046
J. Am. Chem. Soc. 2015, 137, 4288−4291

potential, compared with that on 4.5 nm Pd. The difference of TOF for CO production over differently sized Pd NPs is enlarged at high applied potentials, revealing that the electrochemical step for formation of HCOO* and CO* becomes dominant on the reaction rate. The increase of TOF on 2.4 and 10.3 nm Pd is much less sensitive with the applied potential than that on Pd NPs with the middle sizes (Figure S12a), which suggests that the non-electrochemical step plays very important roles on 2.4 and 10.3 nm Pd, probably associated with the strong adsorption of CO on step and corner sites and weak adsorption of CO_2 on terrace site, respectively. TOF for H_2 production increases with the increasing size of Pd NPs at various potentials (Figures S12b and S13). The formation of H* is similar on corner, edge, and terrace sites and participates in both CO_2 reduction and HER. The increase of TOF values for H_2 production in the size range from 2.4 to 4.5 nm is sluggish because H* on corner and edge sites (small Pd NPs) might mainly participate in the formation of COOH* and CO* in CO_2 reduction. On the contrary, H_2 production increases drastically in the size range from 4.5 to 10.3 nm because H* on terrace site (large Pd NPs) is less influenced by the formation of CO and is converted to H_2 predominantly.

In summary, a unique particle size dependence of Faradaic efficiencies and current densities for CO_2 reduction has been demonstrated over Pd NPs with the narrow size range of 2.4−10.3 nm. DFT calculations found that corner and edge sites on Pd NPs were more active than terrace sites toward CO_2 reduction and that competitive HER was similar on all three sites. The volcano-like curve of TOF for CO production within the size range suggests that CO_2 adsorption, COOH* formation, and CO* removal during CO_2 reduction can be tuned by varying the size of Pd NPs due to the changing ratio of corner, edge, and terrace sites.

■ ASSOCIATED CONTENT

Supporting Information

Experimental details, TEM and HRTEM images, XRD patterns, mass activities for CO production, cyclic voltammograms, and DFT calculation details. This material is available free of charge via the Internet at http://pubs.acs.org.

■ AUTHOR INFORMATION

Corresponding Authors

*wanggx@dicp.ac.cn

*jgw@zjut.edu.cn

Author Contributions

‖D.G. and H.Z. contributed equally.

Notes

The authors declare no competing financial interest.

■ ACKNOWLEDGMENTS

We gratefully acknowledge financial support from the Ministry of Science and Technology of China (Grants 2012CB215500 and 2013CB733501) and the National Natural Science Foundation of China (Grants 21136001, 21103178, and 21176211).

■ REFERENCES

(1) Scott, V.; Gilfillan, S.; Markusson, N.; Chalmers, H.; Haszeldine, R. S. *Nat. Clim. Change* **2012**, *3*, 105.

(2) Yekini Suberu, M.; Wazir Mustafa, M.; Bashir, N. *Renew. Sust. Energy Rev.* **2014**, *35*, 499.

(3) Olah, G. A.; Prakash, G. K.; Goeppert, A. *J. Am. Chem. Soc.* **2011**, *133*, 12881.

(4) Whipple, D. T.; Kenis, P. J. A. *J. Phys. Chem. Lett.* **2010**, *1*, 3451.

(5) Qiao, J.; Liu, Y.; Hong, F.; Zhang, J. *Chem. Soc. Rev.* **2014**, *43*, 631.

(6) Rosen, B. A.; Salehi-Khojin, A.; Thorson, M. R.; Zhu, W.; Whipple, D. T.; Kenis, P. J.; Masel, R. I. *Science* **2011**, *334*, 643.

(7) Tornow, C. E.; Thorson, M. R.; Ma, S.; Gewirth, A. A.; Kenis, P. J. *J. Am. Chem. Soc.* **2012**, *134*, 19520.

(8) Zhang, S.; Kang, P.; Ubnoske, S.; Brennaman, M. K.; Song, N.; House, R. L.; Glass, J. T.; Meyer, T. J. *J. Am. Chem. Soc.* **2014**, *136*, 7845.

(9) Gao, D.; Cai, F.; Xu, Q.; Wang, G.; Pan, X.; Bao, X. *J. Energy Chem.* **2014**, *23*, 694.

(10) Chen, Y.; Kanan, M. W. *J. Am. Chem. Soc.* **2012**, *134*, 1986.

(11) Lu, Q.; Rosen, J.; Zhou, Y.; Hutchings, G. S.; Kimmel, Y. C.; Chen, J. G.; Jiao, F. *Nat. Commun.* **2014**, *5*, 3242.

(12) Peterson, A. A.; Abild-Pedersen, F.; Studt, F.; Rossmeisl, J.; Norskov, J. K. *Energy Environ. Sci.* **2010**, *3*, 1311.

(13) Kas, R.; Kortlever, R.; Milbrat, A.; Koper, M. T.; Mul, G.; Baltrusaitis, J. *Phys. Chem. Chem. Phys.* **2014**, *16*, 12194.

(14) Hori, Y. In *Modern Aspects of Electrochemistry*; Vayenas, C. G., White, R. E., Gamboa-Aldeco, M. E., Eds.; Springer: New York, 2008; Vol. *42*, p 89.

(15) Salehi-Khojin, A.; Jhong, H.-R. M.; Rosen, B. A.; Zhu, W.; Ma, S.; Kenis, P. J. A.; Masel, R. I. *J. Phys. Chem. C* **2013**, *117*, 1627.

(16) Zhang, S.; Kang, P.; Meyer, T. J. *J. Am. Chem. Soc.* **2014**, *136*, 1734.

(17) Reske, R.; Mistry, H.; Behafarid, F.; Roldan Cuenya, B.; Strasser, P. *J. Am. Chem. Soc.* **2014**, *136*, 6978.

(18) Mistry, H.; Reske, R.; Zeng, Z.; Zhao, Z. J.; Greeley, J.; Strasser, P.; Cuenya, B. R. *J. Am. Chem. Soc.* **2014**, *136*, 16473.

(19) Zhu, W.; Michalsky, R.; Metin, O.; Lv, H.; Guo, S.; Wright, C. J.; Sun, X.; Peterson, A. A.; Sun, S. *J. Am. Chem. Soc.* **2013**, *135*, 16833.

(20) Ohkawa, K.; Hashimato, K.; Fujishima, A. *J. Appl. Electrochem.* **1993**, *345*, 445.

(21) Zhu, W.; Zhang, Y. J.; Zhang, H.; Lv, H.; Li, Q.; Michalsky, R.; Peterson, A. A.; Sun, S. *J. Am. Chem. Soc.* **2014**, *136*, 16132.

(22) Lyu, J.; Wang, J.; Lu, C.; Ma, L.; Zhang, Q.; He, X.; Li, X. *J. Phys. Chem. C* **2014**, *118*, 2594.

(23) Durand, W. J.; Peterson, A. A.; Studt, F.; Abild-Pedersen, F.; Nørskov, J. K. *Surf. Sci.* **2011**, *605*, 1354.

(24) Hansen, H. A.; Varley, J. B.; Peterson, A. A.; Nørskov, J. K. *J. Phys. Chem. Lett.* **2013**, *4*, 388.

(25) Xiao, L.; Zhuang, L.; Liu, Y.; Lu, J.; Abruna, H. D. *J. Am. Chem. Soc.* **2009**, *131*, 602.

(26) Mayrhofer, K. J. J.; Blizanac, B. B.; Arenz, M.; Stamenkovic, V. R.; Ross, P. N.; Markovic, N. M. *J. Phys. Chem. C* **2005**, *109*, 14433.

DOI: 10.1021/jacs.5b00046
J. Am. Chem. Soc. 2015, 137, 4288−4291